

Epidemiological and virological update on the emerging SARS-CoV-2 variant BA.3.2

The constant emergence of novel SARS-CoV-2 variants has driven the COVID-19 pandemic and sustains the current endemic. Saltation variants, such as BA.2.86,¹ encode highly mutated spike (S) proteins that efficiently evade neutralising antibodies. In November, 2024, a potential saltation variant, BA.3.2, was detected in South Africa but its spread remained uncertain. Early studies on BA.3.2 did not include comparisons among its subvariants or with dominant variants NB.1.8.1 and XFG.^{2,3} Moreover, the effect of the often overlooked S protein insertion of Ala-Ser-Asp-Thr at position 214 remained unexamined. In this Correspondence, we provide an epidemiological and virological update on BA.3.2, with the use of BA.3 (parental lineage) and NB.1.8.1 and XFG (currently prevalent) as references.

BA.3.2 accounted for five (18%) of 28 sequences reported in South Africa between March and June, 2025, (GISAID EpiCoV database). The variant was detected in Mozambique on March 17, 2025, suggesting its broader spread in sub-Saharan Africa. BA.3.2 was first identified in the Netherlands on April 2, 2025, and in Germany on April 29, followed by its detection in US air travellers from the Netherlands on June 17 (appendix pp 2, 14). The variant later appeared in Australia, where it comprised 8% of wastewater sequences in Perth, Western Australia, from Sept 8 to 14, and 20% from Sept 15 to 21.⁴ Furthermore, BA.3.2 was detected in four (50%) of eight clinical samples in Perth during Sept 15–21, and in one (14%) of seven during Sept 22–28 (appendix pp 2, 14).⁴ For comparison, NB.1.8.1 and XFG began spreading in February and March, 2025, respectively, with

XFG now the globally dominant variant (appendix pp 2, 14).

Two BA.3.2 sublineages (BA.3.2.1 and BA.3.2.2) differ from BA.3.2 by the S protein signature mutations H681R/P1162R and K356T/A575S, respectively, and differ from the BA.3 (wild type) S protein by 53 mutations (appendix p 14). The S proteins of NB.1.8.1 and XFG contain the unique mutations F59S/G184S/V445H/K478I and S31P/K182R/R190S/R346T/K444R/V445R/N487D/T1572I, respectively, and differ from the BA.3 S protein by 51 and 48 mutations, respectively (appendix p 14). We analysed cell-line tropism, ACE2 usage, and neutralisation sensitivity of these variants, with the use of a well established pseudotyping system⁵ and the BA.3 S protein as a reference.

We found that particles pseudotyped with BA.3, BA.3.2.1, and BA.3.2.2 S proteins (ie, BA.3_{pp}, BA.3.2.1_{pp}, and BA.3.2.2_{pp}) entered the Caco-2 human colon cell line and the African green monkey kidney-derived Vero cell line with similar efficiency, as expected,³ and slightly less efficiently compared with XFG_{pp} (Vero) and NB.1.8.1_{pp} (Caco-2; appendix pp 2, 14). In contrast, entry of BA.3.2.1_{pp} and BA.3.2.2_{pp} into Calu-3 and H1299 human lung cell lines was reduced compared with BA.3_{pp}, XFG_{pp}, and, especially, NB.1.8.1_{pp}. These results correlate with weaker ACE2 binding and lower inhibition by recombinant ACE2 (appendix pp 2, 16), which is consistent with previous findings.² Similarly, BA.3.2.1 and BA.3.2.2 S proteins drove less cell-cell fusion than did XFG and NB.1.8.1 S proteins. Furthermore, analysis of plasma samples from individuals vaccinated with the JN.1-based booster vaccine (appendix p 24) revealed that BA.3.2.1_{pp} and BA.3.2.2_{pp} evaded antibodies with higher efficiency than BA.3_{pp}, as expected,³ with the N-terminal domain and the receptor-binding domain accounting for the increased neutralisation resistance (appendix pp 2, 18, 20). Antibody

evasion exceeded that of NB.1.8.1_{pp}, with BA.3.2.2_{pp} being more resistant than BA.3.2.1_{pp} and similarly resistant as XFG_{pp} (appendix pp 2, 20), in agreement with a previous study.²

The strong antibody evasion of BA.3.2 likely results from point mutations in the N1 and N5 loops and a deletion in the N3 loop of the N-terminal domain antigenic supersite, and mutations such as K356T (creating a new sequon) and R403S, R408K, and R493Q, which might alter class 1/4 neutralising antibody epitopes (appendix p 22). Conversely, receptor-binding domain mutations affecting ACE2-contacting residues, including S446D, might underlie the reduced ACE2 binding observed here (appendix p 22). However, confirmation of binding data by independent techniques, such as surface plasmon resonance, is needed. Finally, reduced ACE2 binding correlated with decreased entry into lung-derived but not colon-derived or kidney-derived cells, possibly reflecting lower ACE2 expression in lung cell lines.

As of Oct 13, 2025, BA.3.2 had spread across four continents at low prevalence, with potential for wider global expansion, although enhanced ACE2 binding and lung cell entry are likely prerequisites for such spread. The strain's antibody evasion is similar to that of the highly prevalent XFG variant and, thus, unlikely to constrain BA.3.2's global potential, although a broader spectrum of patients remains to be analysed.

The pronounced spread of BA.3.2.2 in Perth (population ~2 million) and its detection in Sydney on Sept 3, 2025, (EPI_ISL_20187886, GISAID) might allow this variant to gain adaptive mutations. Some Australian viruses now carry unique S protein changes—T259I and P1162L. A sequence deposited on Aug 28, 2025, indicates possible co-infection or recombination between NB.1.8.1 and BA.3.2 (EPI_ISL_20175638). If BA.3.2 spreads globally, it must be assessed whether the upcoming LP.8.1-adapted booster



Lancet Infect Dis 2025

Published Online

November 12, 2025

[https://doi.org/10.1016/S1473-3099\(25\)00658-9](https://doi.org/10.1016/S1473-3099(25)00658-9)

For more on GISAID EpiCoV database see <https://gisaid.org/>

See Online for appendix

vaccines provide sufficient protection, especially for vulnerable groups.

Conceptualisation: LZ, GMNB, MH, and SP. Formal analysis: LZ. Funding acquisition: NC, AD-J, GMNB, and SP. Investigation: LZ, NC, AE, IN, and A-SM. Patient samples and metadata collection: MVS, CH, AD-J, and GMNB. Writing of the original draft: LZ and SP. All authors: review and editing. LZ and SP have directly accessed and verified the underlying data reported in the manuscript. AE, IN, SP, and MH conducted contract research (testing of vaccine sera for neutralising activity against SARS-CoV-2) for Valneva. GMNB was an adviser for Moderna, SP was an adviser for BioNTech, and AD-J was an adviser for Pfizer, all unrelated to this work. All other authors declare no competing interests. During the preparation of this work the authors used ChatGPT (OpenAI) in order to assist with grammar and style corrections. After using this service, the authors reviewed and edited the content as needed and take full responsibility for the content of the publication.

*Lu Zhang, Nianzhen Chen,
Amy Eichmann, Inga Nehlmeier,
Anna-Sophie Moldenhauer,
Metodi V Stankov, Christine Happle,
Alexandra Dopfer-Jablonka,
Georg M N Behrens,
Markus Hoffmann, *Stefan Pöhlmann
spoehlmann@dpz.eu*

Infection Biology Unit, German Primate Center, Göttingen 37077, Germany (LZ, NC, AE, IN, A-SM, MH, SP); Faculty of Biology and Psychology, Georg-August-University Göttingen, Göttingen 37073, Germany (AE, SP); Department for Paediatric Pneumology (CH), Department for Rheumatology and Immunology (MVS, CH, AD-J, GMNB), Hannover Medical School, Hannover, Germany; German Centre for Lung Research, partner site Hannover BREATH, Hannover, Germany (CH); German Centre for Infection Research, partner site Hannover-Braunschweig, Hannover, Germany (MVS, CH, AD-J, GMNB).

- 1 Zhang L, Kempf A, Nehlmeier I, et al. SARS-CoV-2 BA.2.6 enters lung cells and evades neutralizing antibodies with high efficiency. *Cell* 2024; **187**: 596–608.
- 2 Guo C, Yu Y, Liu J, et al. Antigenic and virological characteristics of SARS-CoV-2 variants BA.3.2, XFG, and NB.1.8.1. *Lancet Infect Dis* 2025; **25**: e374–77.
- 3 Zhang L, Kempf A, Nehlmeier I, et al. Host cell entry and neutralisation sensitivity of SARS-CoV-2 BA.3.2. *Lancet Microbe* 2025; published online June 3. <https://doi.org/10.1016/j.lanmic.2025.101165>.
- 4 Government of Western Australia DoH. Respiratory virus wastewater surveillance, SARS-CoV-2 variant lineages. 2025. https://www.health.wa.gov.au/articles/n_r/ respiratory-virus-wastewater-surveillance (accessed Oct 13, 2025).
- 5 Schmidt F, Weisblum Y, Muecksch F, et al. Measuring SARS-CoV-2 neutralizing antibody activity using pseudotyped and chimeric viruses. *J Exp Med* 2020; **217**: e20201181.

THE LANCET

Infectious Diseases

Supplementary appendix

This appendix formed part of the original submission. We post it as supplied by the authors.

Supplement to: Zhang L, Chen N, Eichmann A, et al. Epidemiological and virological update on the emerging SARS-CoV-2 variant BA.3.2. *Lancet Infect Dis* 2025; published online Nov 12. [https://doi.org/10.1016/S1473-3099\(25\)00658-9](https://doi.org/10.1016/S1473-3099(25)00658-9).

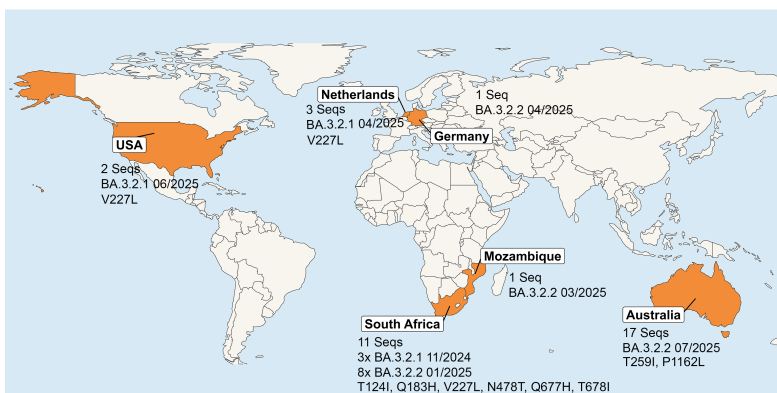
Epidemiology and antigenic profile of the emerging SARS-CoV-2 variant BA.3.2

Contents

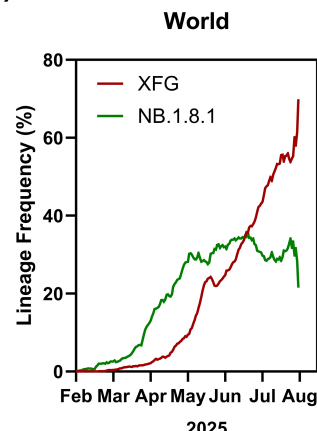
Figure	2
Methods	5
Limitations of the study	11
Acknowledgements	11
Supplementary references	12
Supplementary figure 1	14
Supplementary figure 2	16
Supplementary figure 3	18
Supplementary figure 4	20
Supplementary figure 5	22
Supplementary Table 1:	24

Figure

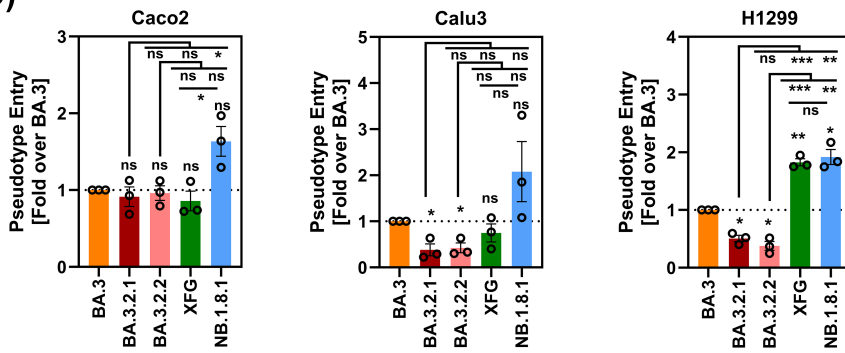
A)



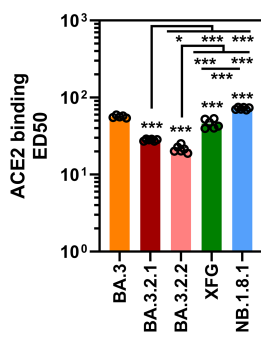
B)



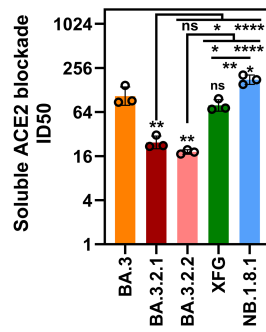
C)



D)



E)



F)

JN.1 booster vaccination

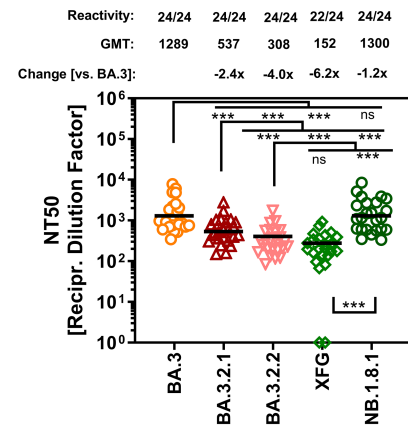


Figure: Epidemiology, cell entry and antibody evasion of emerging SARS-CoV-2 variants

BA.3.2.1 and BA.3.2.2

(A) Global distribution and evolution of SARS-CoV-2 BA.3.2.1 and BA.3.2.2 lineages based on data retrieved from the GISAID EpiCoV™ database (accessed on October 13th 2025). Countries with reported cases of BA.3.2 variants are shown in orange. For each country, information on the

number of available sequences and the date of first detection is provided. Additional spike (S) protein mutations that emerged during the transmission of BA.3.2.1 and BA.3.2.2 are indicated.

(B) Global frequency of SARS-CoV-2 lineages XFG and NB.1.8.1 between February 2025 and August 2025 (data are based on the covSPECTRUM database, <https://cov-spectrum.org/>; accessed on August 20th 2025).

(C) Particles pseudotyped with the indicated S proteins were inoculated onto Caco-2 (human colon), Calu-3 (human lung), Vero (African green monkey kidney), and H1299 (human lung) cells. Cell entry was analysed at 16-18 h post-inoculation by quantifying virus-encoded firefly luciferase activity in cell lysates. Data represent means of three biological replicates, each performed with four technical replicates; error bars show the standard error of the mean (SEM). Results were normalised to cell entry mediated by BA.3 pseudovirus (set as 1, dashed line). Statistical significance was assessed using a two-tailed Student's t test (not significant [ns], $p > 0.05$; *, $p \leq 0.05$; **, $p \leq 0.01$; ***, $p \leq 0.001$). Please also see supplementary figure 1D.

(D) 293T cells expressing the indicated S proteins after transfection were harvested and analysed by flow cytometry for S protein cell-surface expression (see supplementary figure 2D) and binding to serial dilutions of soluble ACE2. Data represent means of six biological replicates (each conducted with a single sample). ACE2 binding efficiency was normalised to the respective S protein incubated with undiluted soluble human ACE2 (set as 100% binding). The effective soluble ACE2 dilution for half-maximal binding signals (ED50) was calculated using linear regression model. Error bars indicate the SEM. Statistical significance was determined by two-way analysis of variance (ANOVA) with Tukey's correction (ns, $p > 0.05$; *, $p \leq 0.05$; **, $p \leq 0.01$; ***, $p \leq 0.001$; Please see also supplementary figure 2C.

(E) Pseudotyped particles bearing the indicated S proteins were pre-incubated with different concentrations of soluble ACE2 and added to Vero cells. Cell entry was analysed at 16-18 h post-inoculation by quantifying virus-encoded luciferase activity, as described above. Data represent normalised means from three biological replicates (each conducted with four technical replicates). Entry in the absence of soluble ACE2 was set as 100%. Further, a non-linear regression model

was used to determine the soluble ACE2 dilution required for half-maximal inhibition (inhibition dilution 50, ID50). Error bars indicate the SEM. Statistical significance was assessed by two-way ANOVA with Tukey's correction (ns, $p > 0.05$; *, $p \leq 0.05$; **, $p \leq 0.01$; ***, $p \leq 0.001$). Please see also supplementary figure 2E.

(F) Neutralisation sensitivity was assessed using plasma collected at 21 days after JN.1 booster vaccination ($n=30$). Pseudotyped particles bearing the indicated S proteins were pre-incubated with serial plasma dilutions and inoculated onto Vero cells. Relative inhibition was calculated using particles incubated without plasma as the control (set as 0% inhibition). Neutralising titre 50 (NT50) values were determined for each plasma sample by a non-linear regression model, and geometric mean titres (GMTs) were calculated for each group. Further, fold changes in neutralisation were calculated using BA.3 pseudovirus particles as reference. Results are based on a single experiment with four technical replicates. Statistical significance was assessed by two-tailed Student's t-test with Welch correction (ns, $p > 0.05$; *, $p \leq 0.05$; **, $p \leq 0.01$; ***, $p \leq 0.001$). Additional information can be found in supplementary figure 3 and supplementary table 1.

Methods

Cell culture

All cell lines were maintained at 37 °C in a humidified atmosphere containing 5% CO₂. Authentication of the cell lines was performed by short tandem repeat (STR) analysis, PCR amplification and sequencing of a cytochrome c oxidase gene fragment, microscopic inspection, and/or cell line-specific growth characteristics. Mycoplasma contamination was excluded by regular PCR-based testing. Vero76 cells (African green monkey kidney, female; CRL-1586, ATCC; RRID: CVCL_0574, kindly provided by Andrea Maisner) and 293T cells (human kidney, female; ACC-635, DSMZ; RRID: CVCL_0063) were grown in Dulbecco's modified Eagle's medium (DMEM; PAN-Biotech) supplemented with 10% fetal bovine serum (FBS, Biochrom) and 1% penicillin-streptomycin solution (pen/strep; PAN-Biotech). Caco-2 cells (human colon, male; HTB-37, ATCC; RRID: CVCL_0025) were cultured in minimum essential medium (MEM; Thermo Fisher Scientific) containing 10% FBS, 1% pen/strep, 1% non-essential amino acid solution (PAA), and 1 mM sodium pyruvate (PAN-Biotech). Calu-3 cells (human lung, male; HTB-55, ATCC; RRID: CVCL_0609, kindly provided by Stephan Ludwig) were maintained in MEM supplemented with 20% FBS, 1% pen/strep, 1% non-essential amino acid solution, and 1 mM sodium pyruvate. NCI-H1299 cells (human lung, male; CRL-5803, ATCC; RRID: CVCL_0060, kindly provided by Christian Drosten) were grown in Roswell Park Memorial Institute (RPMI) 1640 medium (PAN-Biotech) supplemented with 10% FBS, 1% pen/strep, 1% non-essential amino acid solution, and 1 mM sodium pyruvate. Transfection of 293T cells was carried out by calcium phosphate precipitation.

Expression plasmids and sequence analysis

Expression plasmids pCAGGS-DsRed¹, pCAGGS-VSV-G², pCG1-SARS-CoV-2 BA.3 SΔ18 (codon-optimised, C-terminal truncation of 18 amino acid residues)^{3,4}, pCG1_solACE2-Fc⁵, pQCXIP-beta-galactosidase alpha fragment⁴, and pQCXIP-beta-galactosidase omega fragment⁴

have been described previously. Plasmids encoding SARS-CoV-2 BA.3.2.1 SΔ18 and BA.3.2.2 SΔ18 were generated from pCG1-SARS-CoV-2 BA.3.2(A) SΔ18 and pCG1-SARS-CoV-2 BA.3.2(B) SΔ18⁶ (both codon-optimised, C-terminal truncation of 18 residues) by PCR-based introduction of the 214ASDT insertion using overlapping primers carrying the mutation. The SARS-CoV-2 XFG SΔ18 plasmid (EPI_ISL_20053327, codon-optimised, C-terminal truncation of 18 residues) was assembled from two synthetic gene strings (Thermo Fisher) and one PCR-amplified fragment using Gibson assembly. To obtain pCG1-SARS-CoV-2 NB.1.8.1 SΔ18 (EPI_ISL_19826033), the mutations G184S, A435S, K478I, and L1104V were introduced into plasmid pCG1-SARS-CoV-2 XEC SΔ18^{7,8} (codon-optimised, C-terminal truncation of 18 residues) by overlap-extension PCR with overlapping primers that harbour the respective mutations. All S protein plasmid constructs were sequence-verified by Sanger sequencing (Microsynth SeqLab). The pCG1 expression vector was kindly provided by Roberto Cattaneo (Mayo Clinic, Rochester, MN, USA). Information on SARS-CoV-2 lineages and corresponding mutations was retrieved from the GISAID (<https://gisaid.org/>) and CoV-Spectrum (<https://cov-spectrum.org/>) databases on 13th of October and 20th of August 2025, respectively.

Analysis of S protein incorporation into pseudovirus particles

Pseudoviruses carrying the S protein were concentrated by centrifugation at 16,800 g for 90 min at 4 °C through a 20% (w/v) sucrose cushion prepared in PBS. Pseudoviral pellets were lysed in 2x SDS sample buffer (0.03 M Tris-HCl, 10% glycerol, 2% SDS, 5% β-mercaptoethanol, 0.2% bromophenol blue, 1 mM EDTA). Proteins were resolved by SDS-PAGE and transferred onto nitrocellulose membranes (Hartenstein). Membranes were blocked for 30 min in PBS-T (PBS with 0.02% Tween-20; Carl Roth) containing 5% bovine serum albumin (BSA), followed by overnight incubation at 4 °C with primary antibodies against the S2 subunit (rabbit, 1:2000 in PBS-T with 5% BSA; Biozol, SIN-40590-T62) or the VSV matrix protein (mouse, 1:1000 in PBS-T with 5% skim milk; Kerafast, EB0011). After three washes with PBS-T, membranes were incubated with HRP-conjugated secondary antibodies: anti-rabbit (1:2000; Dianova, 111-035-003) or anti-mouse

(1:2000; Dianova, 115-035-003), diluted in PBS-T with 5% skim milk. Blots were washed again three times in PBS-T, and protein bands were detected using a homemade chemiluminescence substrate (0.1 M Tris-HCl [pH 8.6], 250 µg/ml luminol, 0.1 mg/ml para-hydroxycoumaric acid, 0.3% hydrogen peroxide). Signal detection was performed using the Azure 600 imaging system, and data were processed with AzureSpot Pro software (Azure Biosystems).

Pseudovirus particle production

Pseudovirus particles were produced as previously described⁹. Briefly, 293T cells were transfected with plasmids encoding the respective S protein, VSV-G, empty vector (EV, negative control) or DsRed (negative control). At 24 h post-transfection, cells were washed with PBS and inoculated with VSV-G-trans-complemented VSV*ΔG (FLuc) (kindly provided by Gert Zimmer)¹⁰. After 1 h of incubation at 37 °C, cells were washed with PBS and further incubated in culture medium supplemented with anti-VSV-G antibody (supernatant from I1-hybridoma cells; ATCC CRL-2700). Cells transfected with VSV-G plasmid received antibody-free medium. At 16-18 h post-inoculation, supernatants were collected and cleared of cellular debris by centrifugation (4,000 g, 10 min). Clarified pseudovirus preparations were aliquot and stored at -80 °C until further use.

Production of soluble human ACE2-Fc

293T cells were transfected with a plasmid encoding soluble human ACE2 fused to the Fc region of human immunoglobulin G (solACE2-Fc). Ten hours after transfection, the culture medium was replaced, and cells were incubated for an additional 38 h. Supernatants were collected and clarified by centrifugation (2000 g, 10 min, 4 °C) and used directly for soluble ACE2 binding and blocking assays.

S protein-mediated cell entry

To evaluate cell tropism and entry efficiency, equal volumes of pseudotyped VSV particles bearing SARS-CoV-2 S proteins, VSV-G (positive control), or lacking glycoprotein (negative control) were inoculated onto target cells seeded in 96-well plates. To assess inhibition by soluble ACE2, pseudoviruses were pre-incubated at 37 °C for 30-60 min with equal volumes of serial solACE2-Fc dilutions (undiluted, 1:4, 1:16, 1:64, 1:256, 1:1024, 1:4096) or with diluent only (culture medium, control) before inoculation. At 16-18 h post-inoculation, viral entry was quantified by measuring firefly luciferase activity encoded by the pseudovirus genome. For detection, culture medium was removed and cells were lysed in PBS containing 0.5% Tergitol 15-S-9 (Carl Roth) for 30 min at room temperature (50µl/well). Lysates were transferred into white 96-well plates, mixed with an equal volume of luciferase substrate (Beetle-Juice, PJK), and luminescence was measured using a Hidex Sense luminometer (Hidex).

ACE2 binding and S protein surface expression assay

At 24 h post-transfection, the medium was replaced with fresh medium and cells were further incubated. At 48 h post-transfection, cells were washed with PBS and resuspended in PBS-B (PBS supplemented with 1% bovine serum albumin [BSA]; Carl Roth). For staining, cell pellets were resuspended in 100 µl PBS-B containing either anti-SARS-CoV-2 S2 antibody (for S protein surface expression; 1:200, GeneTex, 1A9) or serial dilutions of solACE2-Fc (undiluted, 1:4, 1:16, 1:64, 1:256, 1:1024, 1:4096, 1:16384). Samples were incubated for 1 h at 4 °C on a Rotospin test tube rotator disk (IKA). Following incubation, cells were pelleted (600 x g, 5 min, room temperature), washed with PBS-B, and resuspended in 100 µl PBS-B containing either Alexa Fluor 488-conjugated anti-human antibody (1:200; Thermo Fisher Scientific, A-11013) for soluble ACE2 binding, or Alexa Fluor 488-conjugated anti-mouse antibody (1:200; Thermo Fisher Scientific, A-10667) for S protein surface expression. Cells were incubated for 60 min at 4 °C, pelleted again (600 x g, 5 min, room temperature), washed twice with PBS-B, and fixed in 250 µl of 1% paraformaldehyde for 30 min at room temperature. After fixation, cells were pelleted (600 x g, 5 min, room temperature), washed with PBS-B, and finally resuspended in 100 µl PBS-B. ACE2

binding and S protein surface expression were analysed using the ID7000 Spectral Cell Analyzer and ID7000 software (Sony Biotechnology, San Jose, CA, USA).

Cell-cell fusion assay

Cell-cell fusion was analysed as described^{1,4,11-13}. Briefly, effector 293T cells were transfected with beta-galactosidase alpha fragment expression plasmid jointly with plasmids coding for the respective S protein, Nipah virus fusion and glycoprotein (NiV-F, NiV-G; positive control), or empty vector (negative control). In addition, target 293T cells were co-transfected with plasmid encoding for the beta-galactosidase omega fragment jointly with human ACE2 expression alone or in combination with TMPRSS2 expression plasmid. Following 18 h of incubation, both effector and target cells were washed with PBS and maintained in fresh medium for 6 h. Target cells were subsequently resuspended in fresh medium and added onto effector cells. After 18 h of co-culture, Gal-Screen substrate (Thermo Fisher Scientific) was applied, and luminescence was measured 90 min later with a Hidex Sense luminometer.

Neutralization assay

Neutralization assays were conducted as previously described⁴. Briefly, pseudovirus particles were incubated at 37 °C for 30 min with serial dilutions of plasma (1:50, 1:200, 1:800, 1:3200, 1:12,800, 1:51,200). Pseudoviruses incubated without plasma served as a control. Following incubation, pseudovirus-plasma mixtures were added to Vero cells seeded in 96-well plates. After 16-18 h, viral entry was quantified by measuring luciferase activity in cell lysates, as described previously^{1,4,5,7-9,11-17}. Neutralization efficiency was determined as the relative reduction in luciferase activity compared to signals obtained for cells inoculated with pseudovirus that were not exposed to plasma (defined as 0% neutralization). Dose-response curves were generated by a non-linear regression model to calculate the individual 50% neutralising titres (NT50) for each pseudovirus-plasma combination. Plasma samples that failed to reach an NT50 of 6.25 were considered non-neutralising and assigned a value of 1.

Plasma samples

Plasma was obtained from donors (n=30) 21 days after vaccination with the Comirnaty® Omicron JN.1/bretovameran vaccine. Donors reported no SARS-CoV-2 infection between vaccination and sample collection, which was corroborated by the absence of self-reported positive rapid antigen or PCR tests, together with negative or declining anti-nucleocapsid protein (NCP) IgG titres. Prior to neutralization assays, plasma samples were heat-inactivated at 56 °C for 30 min. Detailed donor characteristics are summarised in Supplementary Table 1.

Protein structure analysis and modelling

The BA.3 RBD was modelled using the SWISS-MODEL online tool (<https://swissmodel.expasy.org/>) and the crystal structure PDB: 6XDG¹⁸ as template. Structure analysis and colouring was further done using the UCSF Chimera software version 1.17.3¹⁹.

Ethics approval

Plasma collection and analysis were conducted within the framework of the COVID-19 Contact (CoCo) Study (DRKS00021152), a prospective observational cohort approved by the Institutional Review Board of Hannover Medical School (approval no. 8973_BO_K_2020). The study monitors IgG antibody levels and immune responses in healthcare workers and individuals with potential exposure to SARS-CoV-2 at Hannover Medical School. Written informed consent was obtained from all participants prior to enrolment, and no financial compensation was provided.

Data analysis

Data analysis was conducted using Microsoft Excel (Office Professional Plus 2016; Microsoft Corporation) and GraphPad Prism version 10.6.0 (GraphPad Software). Statistical significance was determined using two-way ANOVA with Tukey's post-hoc test, Wilcoxon matched-pairs test,

or two-tailed Student's t-test with Welch correction. P values ≤ 0.05 were considered statistically significant (ns, p > 0.05; *, p ≤ 0.05 ; **, p ≤ 0.01 ; ***, p ≤ 0.001).

Limitations of the study

This study has several limitations. First, SARS-CoV-2 host cell entry and neutralisation were analysed using S protein-bearing pseudovirus particles, as clinical SARS-CoV-2 isolates were not available. Thus, confirmation of these findings with authentic SARS-CoV-2 isolates and primary cell cultures remains necessary. Second, the relatively small sample size of the cohort precluded analysis of potential biological factors, such as age or biological sex, on neutralisation outcomes. Third, plasma samples were collected 21 days after JN.1 booster vaccination, and the durability of protective immunity beyond this time point remains to be determined.

Acknowledgements

We acknowledge the originating laboratories responsible for sample collection and the submitting laboratories that generated and shared genome data via GISAID, which formed the basis of this study. We thank the participants of the CoCo Study for their contribution, as well as the entire CoCo Study team for their continued support, and we thank Ryan Hisner (@LongDesertTrain), Federico Gueli and Mike Honey (@Mike_Honey) for sharing information on BA.3.2.

AD-J acknowledges funding by the European Social Fund (ZAM5-87006761), and together with GMNB, by the COVID-19-Research Network Lower Saxony (COFONI) through funding from the Ministry of Science and Culture of Lower Saxony in Germany (14-76103-184, project 4LZF23).

SP acknowledges funding by the EU project UNDINE (grant agreement number 101057100), the COVID-19-Research Network Lower Saxony (COFONI) through funding from the Ministry of Science and Culture of Lower Saxony in Germany (14-76403-184, projects 7FF22, 6FF22, 10FF22) and Bundesministerium für Bildung und Forschung (COVIM 2.0, 01KX2121). NC acknowledges funding by the Chinese Scholarship Council (202308310035). The funding sources had no role in the design and execution of the study, writing of the manuscript, or the decision to

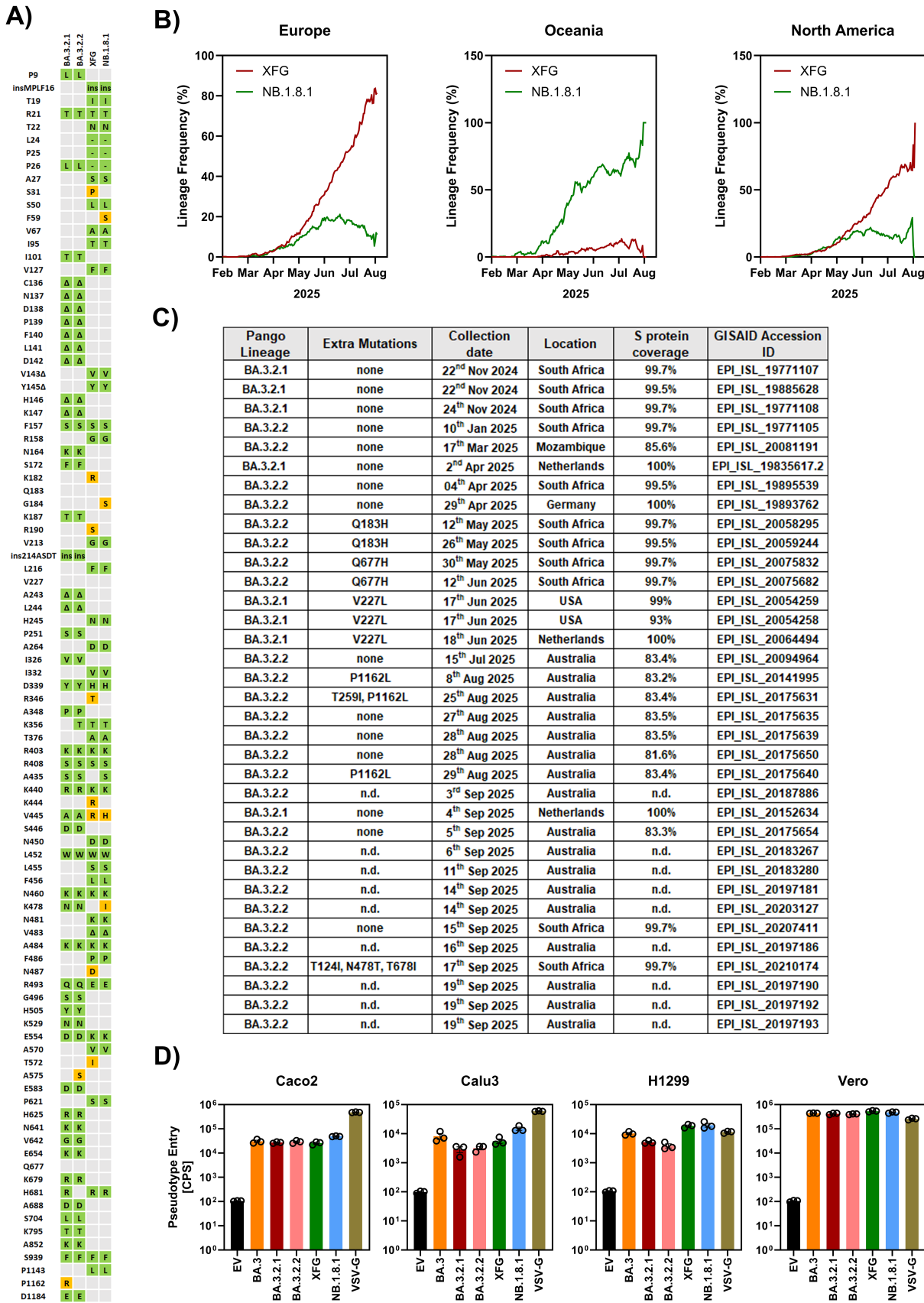
submit the manuscript for publication. The authors did not receive payment from any pharmaceutical company or other agency to write the manuscript. The authors were not precluded from accessing data in the study, and they accept responsibility for submitting it for publication.

Supplementary references

1. Hoffmann M, Kleine-Weber H, Schroeder S, et al. SARS-CoV-2 Cell Entry Depends on ACE2 and TMPRSS2 and Is Blocked by a Clinically Proven Protease Inhibitor. *Cell* 2020; **181**(2): 271-80 e8.
2. Brinkmann C, Hoffmann M, Lubke A, et al. The glycoprotein of vesicular stomatitis virus promotes release of virus-like particles from tetherin-positive cells. *PLoS One* 2017; **12**(12): e0189073.
3. Arora P, Zhang L, Rocha C, et al. Comparable neutralisation evasion of SARS-CoV-2 omicron subvariants BA.1, BA.2, and BA.3. *Lancet Infect Dis* 2022; **22**(6): 766-7.
4. Arora P, Zhang L, Kruger N, et al. SARS-CoV-2 Omicron sublineages show comparable cell entry but differential neutralization by therapeutic antibodies. *Cell Host Microbe* 2022; **30**(8): 1103-11 e6.
5. Hoffmann M, Zhang L, Kruger N, et al. SARS-CoV-2 mutations acquired in mink reduce antibody-mediated neutralization. *Cell Rep* 2021; **35**(3): 109017.
6. Zhang L, Kempf A, Nehlmeier I, et al. Host cell entry and neutralisation sensitivity of SARS-CoV-2 BA.3.2. *Lancet Microbe* 2025: 101165.
7. Arora P, Kempf A, Nehlmeier I, et al. Entry Efficiency, Protease Dependence, and Antibody-Mediated Neutralization of SARS-CoV-2 Sublineages KP.3.1.1 and XEC. *Vaccines (Basel)* 2025; **13**(4).
8. Arora P, Happle C, Kempf A, et al. Impact of JN.1 booster vaccination on neutralisation of SARS-CoV-2 variants KP.3.1.1 and XEC. *Lancet Infect Dis* 2024; **24**(12): e732-e3.
9. Kleine-Weber H, Elzayat MT, Wang L, et al. Mutations in the Spike Protein of Middle East Respiratory Syndrome Coronavirus Transmitted in Korea Increase Resistance to Antibody-Mediated Neutralization. *J Virol* 2019; **93**(2).
10. Berger Rentsch M, Zimmer G. A vesicular stomatitis virus replicon-based bioassay for the rapid and sensitive determination of multi-species type I interferon. *PLoS One* 2011; **6**(10): e25858.
11. Hoffmann M, Arora P, Gross R, et al. SARS-CoV-2 variants B.1.351 and P.1 escape from neutralizing antibodies. *Cell* 2021; **184**(9): 2384-93 e12.
12. Zhang L, Kempf A, Nehlmeier I, et al. SARS-CoV-2 BA.2.86 enters lung cells and evades neutralizing antibodies with high efficiency. *Cell* 2024; **187**(3): 596-608 e17.

13. Hoffmann M, Kruger N, Schulz S, et al. The Omicron variant is highly resistant against antibody-mediated neutralization: Implications for control of the COVID-19 pandemic. *Cell* 2022; **185**(3): 447-56 e11.
14. Zhang L, Kempf A, Nehlmeier I, et al. Host cell entry and neutralisation sensitivity of the emerging SARS-CoV-2 variant LP.8.1. *Lancet Infect Dis* 2025; **25**(4): e196-e7.
15. Zhang L, Dopfer-Jablonka A, Cossmann A, et al. Rapid spread of the SARS-CoV-2 JN.1 lineage is associated with increased neutralization evasion. *iScience* 2024; **27**(6): 109904.
16. Zhang L, Cheng HH, Kruger N, et al. ACE2-independent sarbecovirus cell entry can be supported by TMPRSS2-related enzymes and can reduce sensitivity to antibody-mediated neutralization. *PLoS Pathog* 2024; **20**(11): e1012653.
17. Arora P, Sidarovich A, Kruger N, et al. B.1.617.2 enters and fuses lung cells with increased efficiency and evades antibodies induced by infection and vaccination. *Cell Rep* 2021; **37**(2): 109825.
18. Lan J, Ge J, Yu J, et al. Structure of the SARS-CoV-2 spike receptor-binding domain bound to the ACE2 receptor. *Nature* 2020; **581**(7807): 215-20.
19. Pettersen EF, Goddard TD, Huang CC, et al. UCSF Chimera--a visualization system for exploratory research and analysis. *J Comput Chem* 2004; **25**(13): 1605-12.

Supplementary Figure 1



Supplementary Figure 1: Sequence, prevalence and cell entry of BA.3.2.1 and BA.3.2.2.

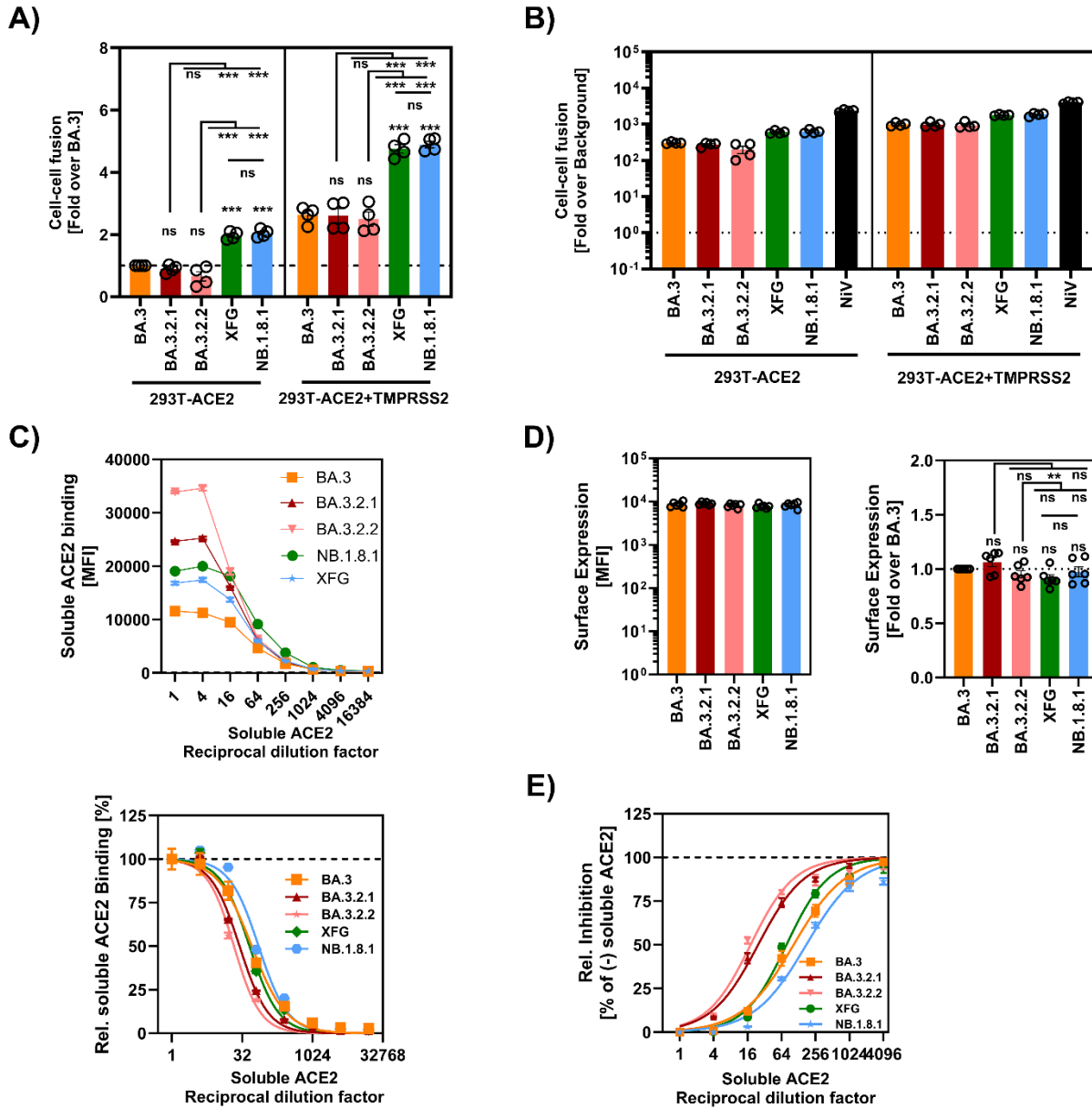
(A) Mutations in the S proteins of SARS-CoV-2 lineages BA.3.2.1, BA.3.2.2, XFG, NB.1.8.1 compared to the S protein of BA.3. Mutation highlighted in orange indicate lineage-specific unique mutations.

(B) Relative frequency of SARS-CoV-2 lineages NB.1.8.1 and XFG in Europe, Oceania and North America (data are based on the covSPECTRUM database, <https://cov-spectrum.org/>; accessed on 20th of August 2025).

(C) Mutations and geographic distribution of available BA.3.2.1 and BA.3.2.2 sequences (data are based on the information obtained from the GISAID EpiCoV™ database, accessed on 13th of October 2025). Of note, for some sequences, poor sequence quality precluded analysis of S protein mutations and sequence coverage (indicated by n.d. = not determinable).

(D) Cell line tropism and entry efficiency of the SARS-CoV-2 lineages BA.3, BA.3.2.1, BA.3.2.2, XFG and NB.1.8.1. Pseudotype particles harbouring the indicated S proteins, VSV-G (vesicular stomatitis glycoprotein; positive control) or no viral glycoprotein (empty vector, EV; negative control) were inoculated onto the indicated cell lines and pseudovirus entry was analysed at 16–18 h postinoculation. Data represent the mean of three biological replicates (conducted with four technical replicates). Error bars indicate the standard deviation (SD). The unprocessed luminescence signals (cps, counts per seconds) for the data presented in figure 1C are shown.

Supplementary Figure 2



Supplementary Figure 2: Cell-cell fusion and ACE2 binding of BA.3.2.1 and BA.3.2.2 S proteins.

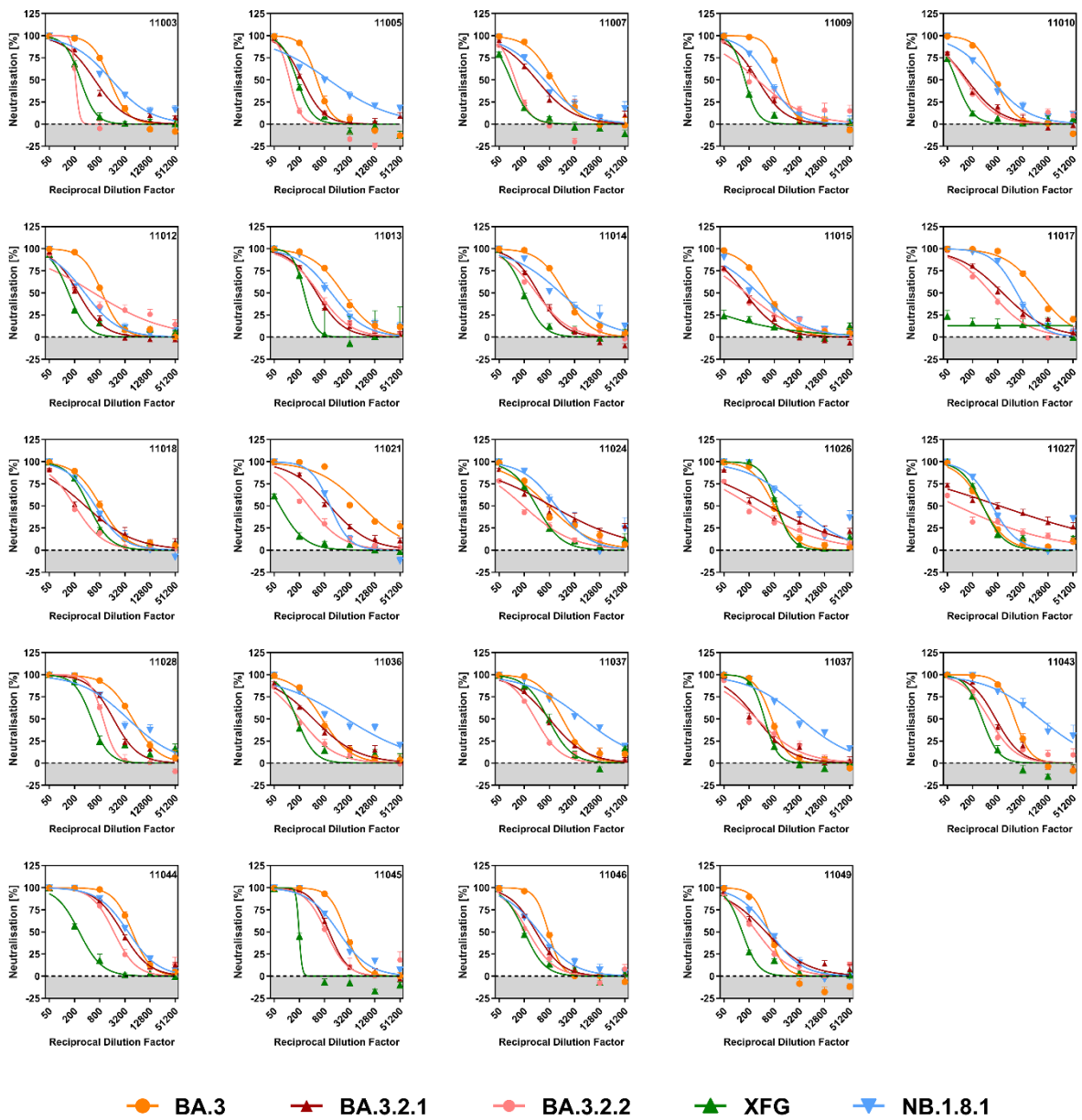
(A) and (B) Cell-cell fusion driven by the BA.3, BA.3.2.1, BA.3.2.2, XFG and NB.1.8.1 S proteins. 293T effector cells expressing the beta-galactosidase alpha fragment and the indicated S protein, Nipah virus fusion- and glycoprotein (NiV-F+G), or no viral glycoprotein (control effector cells) were co-incubated with 293T target cells expressing the beta-galactosidase omega fragment,

ACE2 and no protease or TMPRSS2. Efficiency of cell-cell fusion was determined by quantification of beta-galactosidase activity in cell lysates and data were normalized against signals obtained for effector cells expressing BA.3 and target cells expressing ACE2 but not TMPRSS2 (set as 1). Data show the mean of three biological replicates (each conducted with four technical replicates). Error bars represent the SEM and one-way ANOVA with Tukey's post-hoc test was used to assess statistical significance ($p > 0.05$ = not significant [ns], $p \leq 0.05$ = *, $p \leq 0.01$ = **, $p \leq 0.001$ = ***). For Panel B, signals were normalized against the assay background (signals obtained for control effector cells that were co-incubated with target cells).

(C) and (D) 293T cells expressing the indicated S proteins after transfection were analysed by flow cytometry to determine binding to soluble ACE2 (C) and S protein surface expression (D). Each dataset is presented as unprocessed values (MFI, mean fluorescence intensity) and as normalised values. Data represent means of six biological replicates (each conducted with single samples). For normalisation of ACE2 binding (C, bottom panel), samples incubated with undiluted soluble human ACE2 were set as 100% binding efficiency. Surface expression was normalised to BA.3 (set at 1; D, left panel). Error bars indicate the SEM and one-way ANOVA with Tukey's post-hoc test was used to assess statistical significance ($p > 0.05$ = not significant [ns], $p \leq 0.05$ = *, $p \leq 0.01$ = **, $p \leq 0.001$ = ***).

(E) Pseudotyped particles bearing the indicated S proteins were pre-incubated with different concentrations of soluble ACE2 and added to Vero cells. Cell entry was analysed 16-18 h post-inoculation by quantifying virus-encoded luciferase activity, as described above. Data represent normalised means from three biological replicates (each conducted with four technical replicates). Entry in the absence of soluble ACE2 was set at 100%. Error bars indicate the SEM.

Supplementary Figure 3

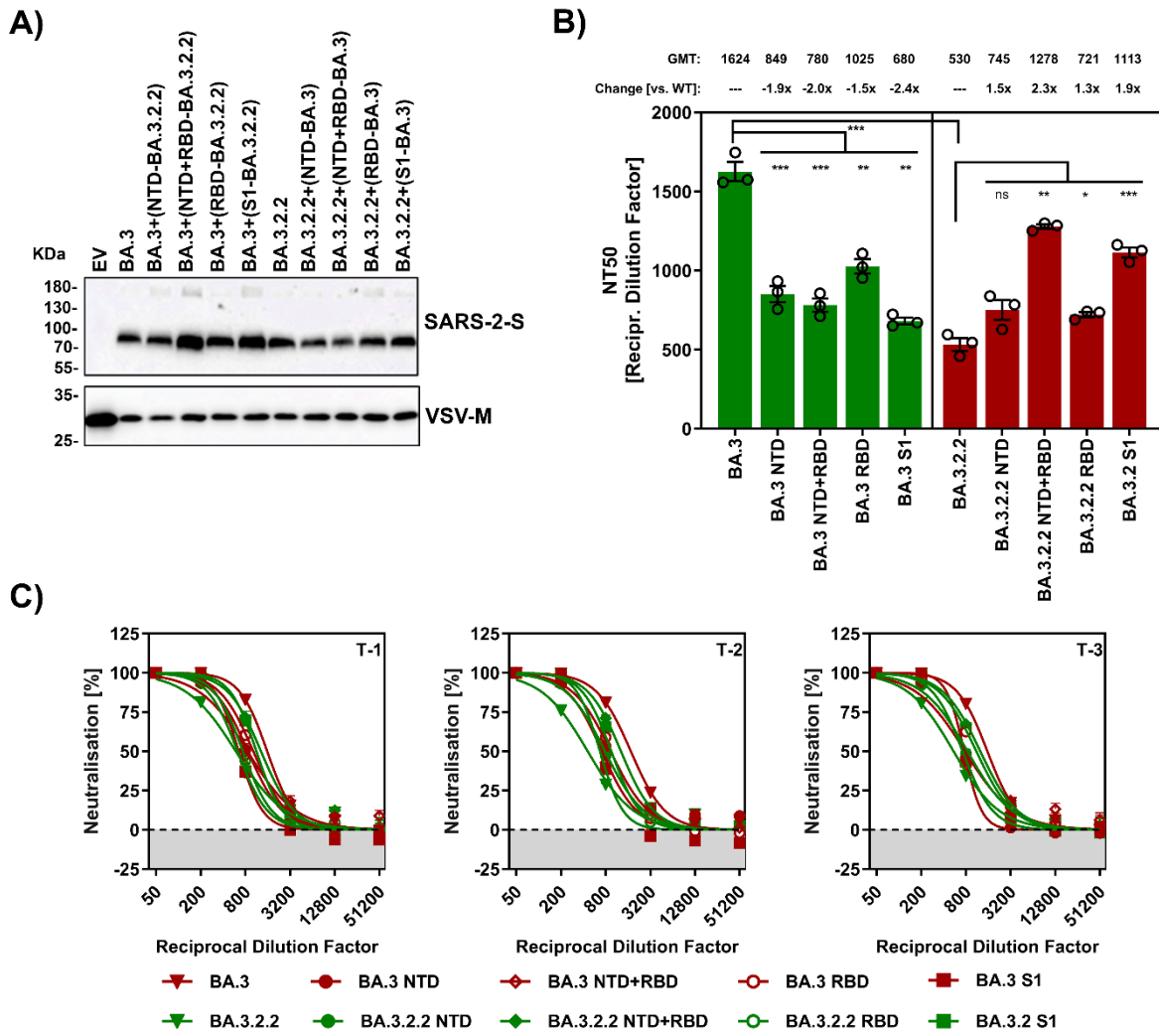


Supplementary Figure 3: Neutralization of BA.3_{pp}, BA.3.2.1_{pp}, BA.3.2.2_{pp}, XFG_{pp}, NB.1.8.1_{pp} by plasma antibodies.

Individual data on BA.3_{pp}, BA.3.2.1_{pp}, BA.3.2.2_{pp}, XFG_{pp}, and NB.1.8.1_{pp} neutralisation by plasma antibodies post JN.1 booster vaccination. Pseudotyped particles bearing the indicated S proteins were pre-incubated with serial plasma dilutions and inoculated onto Vero cells; particles incubated without plasma served as controls. Cell entry was quantified by measuring virus-encoded luciferase activity in cell lysates. The results were normalized to signals for pseudotype particles

that were not incubated with plasma (set as 0% neutralisation). Data represent means from a single experiment with four technical replicates. Error bars indicate the SEM. Curve-fitting was done using a non-linear regression model.

Supplementary Figure 4



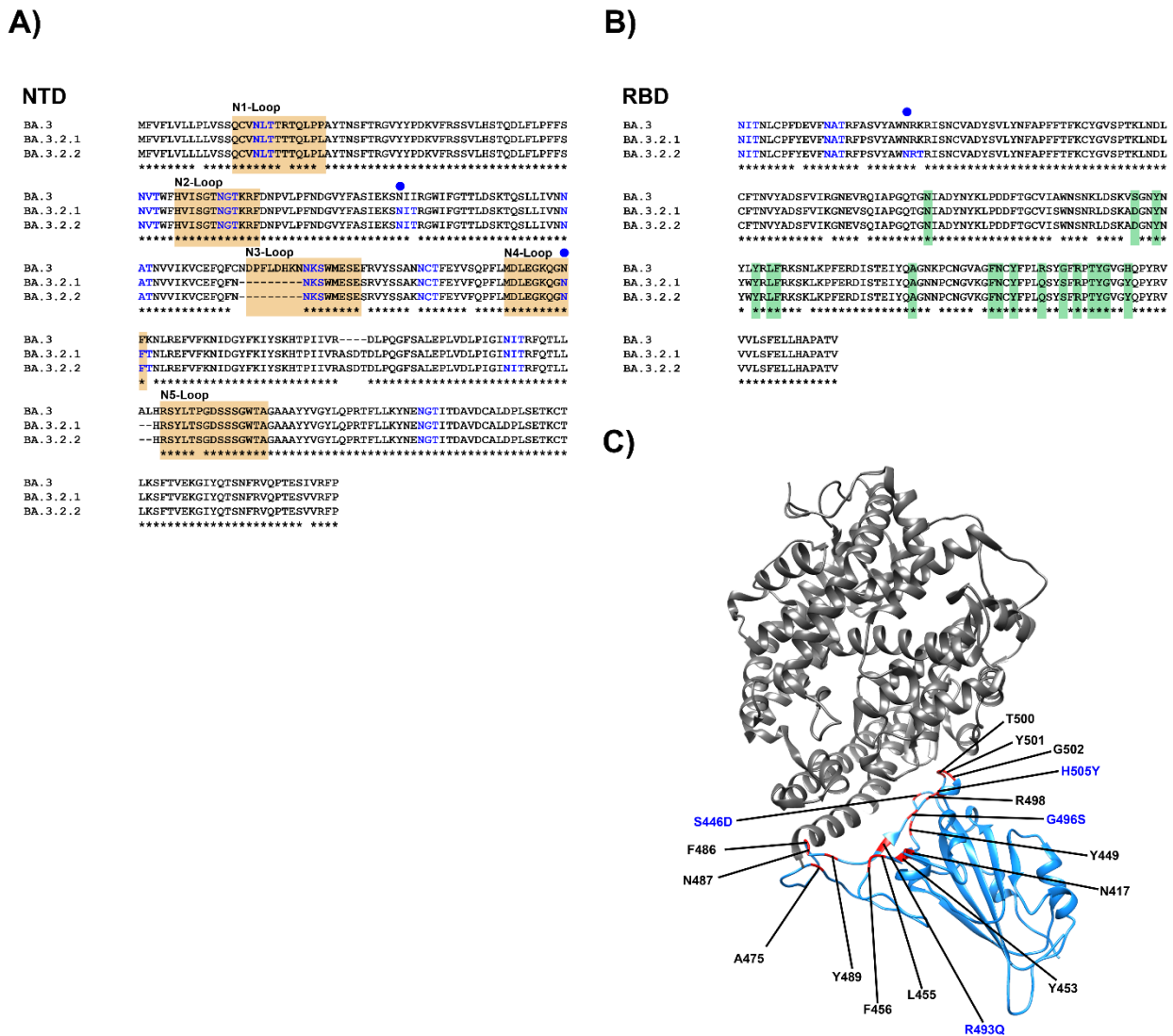
Supplementary Figure 4: Both NTD and RBD contribute to the increased antibody evasion capacity of BA.3.2.2.

(A) Chimeric S proteins were generated by exchanging fragments corresponding to the N-terminal domain (NTD), receptor-binding domain (RBD), NTD and RBD (NTD+RBD), or the whole S1 subunit (S1) between BA.3 and BA.3.2.2 S proteins. Pseudotyped particles were harvested, concentrated through a sucrose cushion, and subjected to SDS-PAGE analysis to analyse S protein particle incorporation. S proteins were detected using antibodies specific for the S2 subunit of SARS-CoV-2 S. In addition, detection of VSV-M (vesicular stomatitis virus matrix protein) served as loading control.

(B) Neutralisation was assessed using a pooled plasma mix from the same donor samples analysed individually in Figure 1E. Pseudotyped particles bearing the indicated S proteins were pre-incubated with serial plasma dilutions and inoculated onto Vero cells. Relative inhibition was calculated using particles incubated without plasma as controls (set as 0% neutralisation). NT50 values were determined by a non-linear regression model, and GMTs were calculated for each group. Data represent means from three biological replicates (each conducted with four technical replicates). Statistical significance was assessed using two-tailed Student's t test with Welch's correction (ns, $p>0.05$; *, $p\leq0.05$; **, $p\leq0.01$; ***, $p\leq0.001$).

(C) Individual neutralisation data for each biological replicate (corresponding to panel B)

Supplementary Figure 5



Supplementary Figure 5. BA.3.2.1/BA.3.2.2-specific mutations in the NTD and RBD.

(A) Alignment of the NTD between BA.3, BA.3.2.1 and BA.3.2.2. Conserved amino acid residues are indicated by asterisks. N-glycosylation motifs are shown in blue with novel N-glycosylation motifs in BA.3.2.1/BA.3.2.2 highlighted by blue circles. Amino acid residues that form the five loops structures (N1-N5) of the NTD supersite are indicated by orange boxes.

(B) Alignment of the RBD between BA.3, BA.3.2.1 and BA.3.2.2. Conserved amino acid residues are indicated by asterisks. N-glycosylation motifs are shown in blue with a novel N-glycosylation motif in BA.3.2.2 highlighted by a blue circle. RBD residues that are known to directly contact ACE2 are indicated by green boxes.

(C) Model structure of the BA.3 spike receptor-binding domain (RBD, light blue) and ACE2 (grey), in which ACE2-interacting residues are marked in red and indicated. BA.3.2.1/BA.3.2.2-specific mutations in ACE2-interacting residues are highlighted in blue.

Supplementary Table 1:
Demographics, and infection and vaccination history

Variable	Vaccinees
Study participants (n=)	24
Age, Median [IQR] (years)	44·5 [8·25]
Sex, male (%)	10 (41·6)
Median time post last vaccination [IQR] (months)	11 [5·1]
Median number of prior vaccinations [IQR]	5 [1]
Prior SARS-CoV-2 omicron vaccination (%)	83·3
Prior SARS-CoV-2 infection (%)	87
Prior SARS-CoV-2 omicron infection (%)	86·3
Prior SARS-CoV-2 omicron antigen contact (%)	100

Abbreviation: IQR, interquartile range